Editors' Suggestion

Instability of Magnetic Skyrmion Strings Induced by Longitudinal Spin Currents

Shun Okumura,[1] Volodymyr P. Kravchuk,[2,3] and Markus Garst[2,4]
[1]Department of Applied Physics, the University of Tokyo, Tokyo 113-8656, Japan
[2]Institut für Theoretische Festkörperphysik, Karlsruher Institut für Technologie, D-76131 Karlsruhe, Germany
[3]Bogolyubov Institute for Theoretical Physics of National Academy of Sciences of Ukraine, 03143 Kyiv, Ukraine
[4]Institute for Quantum Materials and Technology, Karlsruhe Institute of Technology, D-76131 Karlsruhe, Germany

(Received 15 March 2023; revised 13 June 2023; accepted 11 July 2023; published 9 August 2023)

It is well established that spin-transfer torques exerted by in-plane spin currents give rise to a motion of magnetic skyrmions resulting in a skyrmion Hall effect. In films of finite thickness or in three-dimensional bulk samples the skyrmions extend in the third direction forming a string. We demonstrate that a spin current flowing longitudinally along the skyrmion string instead induces a Goldstone spin wave instability. Our analytical results are confirmed by micromagnetic simulations of both a single string as well as string lattices, suggesting that the instability eventually breaks the strings. A longitudinal current is thus able to melt the skyrmion string lattice via a nonequilibrium phase transition. For films of finite thickness or in the presence of disorder a threshold current will be required, and we estimate the latter assuming weak collective pinning.

DOI: 10.1103/PhysRevLett.131.066702

One of the fascinating aspects of two-dimensional topological spin textures, so-called magnetic skyrmions, is their interplay with spin currents [1]. When electrons adiabatically traverse a skyrmion and locally adjust their spin degree of freedom, they will be influenced by an emergent orbital magnetic field that is proportional to the topological winding number of the texture [2]. The resulting emergent Lorentz force is at the origin of the topological Hall effect [3–5]. Vice versa, a spin current also exerts a force on skyrmions that gives rise to a skyrmion Hall effect. Early experiments demonstrated that a lattice of magnetic skyrmions in bulk chiral magnets like MnSi and FeGe can be manipulated by currents on the order of an ultralow threshold of 10^6 A/m^2 [6–8]. This observation triggered many activities with the aim to exploit magnetic skyrmions for spintronic applications [9–11]. In thin magnetic films, skyrmions are now routinely manipulated and moved by spin currents that flow within the plane of the film [12–19].

In bulk materials, the two-dimensional skyrmion texture extends in the third direction forming a skyrmion string, see Fig. 1(a). This string is aligned with the applied magnetic field and possesses a tension. Recent advances in real-space magnetic imaging techniques succeeded to visualize skyrmion strings close to surfaces [20–24] and via magnetic x-ray tomography even within the bulk [25]. Similar to Kelvin waves on vortex filaments, spin waves can propagate along skyrmion strings [26], and this propagation is nonreciprocal as confirmed experimentally [27]. Moreover, the nonlinear elasticity of skyrmion strings was found to stabilize solitary waves [28] whose analogs for vortex filaments were discussed by Hasimoto already in the 1970s [29].

The influence of a transversal spin current on skyrmion strings, i.e., a current that flows perpendicular to the string, has been also widely investigated. In analogy with the two-dimensional case, a transversal current density homogeneously applied along the whole string will set the string into motion at least in the absence of pinning by disorder. There exist theoretical [37] and experimental [38]

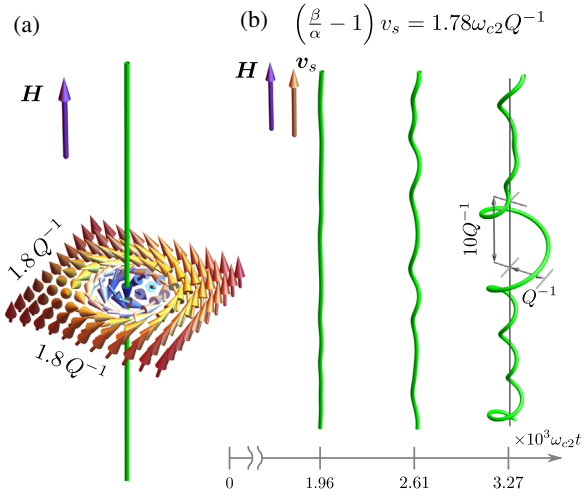

FIG. 1. (a) Illustration of a skyrmion string that is aligned with the applied magnetic field H; each cross section perpendicular to H contains a skyrmion texture, and the green line represents the first moment of topological charge. (b) Micromagnetic simulation of a string destabilized by a longitudinal spin current v_s; after initialization with small random fluctuations the amplitudes of translational Goldstone modes grow exponentially in time, for details see text and Ref. [30].

evidences that pulses of such currents are able to break the strings via the creation of hedgehog singularities, i.e., emergent magnetic monopoles, that lead to a topological unwinding of strings. It has been argued that the complex dynamical response of skyrmion strings results in a nonreciprocal nonlinear Hall effect [39]. The influence of defects on the motion of skyrmion strings was studied in Refs. [40–43], and their elasticity was shown to be important for an understanding of the depinning transition [44].

In the present work, we investigate the influence of spin currents that flow parallel, i.e., longitudinal to the skyrmion string. We show that, remarkably, such a current component immediately destabilizes the string in a clean system. This instability is caused by the longitudinal current leading to the emission of translational Goldstone modes with finite wave vectors along the string, $k_z \neq 0$, in contrast to the transversal current that couples only to the Goldstone mode with $k_z = 0$. As a result, helical deformations develop, see Fig. 1(b), whose amplitudes grow with time and eventually break the string [45]. Employing an analytical stability analysis complemented by micromagnetic simulations, we demonstrate that a single string as well as a skyrmion string lattice are destabilized by this mechanism.

Our starting point is the Landau-Lifshitz-Gilbert equation describing the magnetization dynamics supplemented by spin-transfer torques [46,47]

$$(\partial_t + \boldsymbol{v}_s\boldsymbol{\nabla})\boldsymbol{n} = -\gamma \boldsymbol{n}\times\boldsymbol{B}_{\text{eff}} + \alpha\boldsymbol{n}\times\left(\partial_t + \frac{\beta}{\alpha}\boldsymbol{v}_s\boldsymbol{\nabla}\right)\boldsymbol{n}. \tag{1}$$

The continuous unit vector field $\boldsymbol{n} = \boldsymbol{n}(\boldsymbol{r}, t)$ specifies the local orientation of the magnetization, $\gamma > 0$ is the gyromagnetic ratio, $\alpha > 0$ is the Gilbert damping, and β is the dissipative spin-torque parameter. The spin-transfer torques involve the effective spin velocity $\boldsymbol{v}_s$ that is parallel to the applied spin current density. The effective magnetic field, $\boldsymbol{B}_{\text{eff}} = -(1/M_s)(\delta V/\delta \boldsymbol{n})$ with the saturation magnetization M_s, is determined by the potential $V = \int d\boldsymbol{r}\mathcal{V}$. The potential density for a cubic chiral magnet in the limit of small spin-orbit coupling is given by $\mathcal{V} = \mathcal{V}_0 + \mathcal{V}_{\text{dip}}$, where

$$\mathcal{V}_0 = A(\partial_i \boldsymbol{n})^2 + D\boldsymbol{n}(\boldsymbol{\nabla}\times\boldsymbol{n}) - \mu_0 M_s H n_z, \tag{2}$$

with the exchange stiffness A, the Dzyaloshinskii-Moriya interaction D, the magnetic constant μ_0, and the magnetic field H applied along the z axis. In the following, we choose a right-handed magnetic system $D > 0$. The part $\mathcal{V}_{\text{dip}}$ comprises dipolar interactions. (The latter was neglected only for the results in Fig. 2.) It is convenient to introduce the scales $\omega_{c2} = \gamma D^2/(2AM_s)$ and $Q = D/(2A)$ for frequency and wave vector, respectively, as well as the dimensionless magnetic field $h = \gamma\mu_0 H/\omega_{c2}$. The strength of dipolar interactions is quantified by the parameter $\gamma\mu_0 M_s/\omega_{c2}$ that we fixed to a value 1.3 typical for cubic chiral magnets [48].

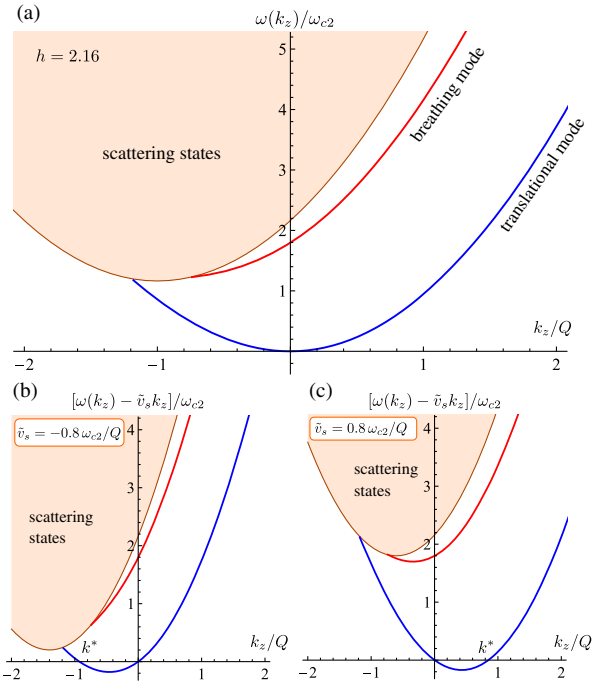

FIG. 2. (a) Spin wave spectrum of a single skyrmion string at $h = 2.16$, neglecting dipolar interaction see Refs. [26,28] for details, consisting of the translational Goldstone mode, the breathing mode, and extended scattering states. (b),(c) In the presence of a small longitudinal current $v_s \neq 0$, the stability criterion (4) is violated for the translational Goldstone mode with wave vectors from zero to k^* for which $\omega(k_z) - \tilde{v}_s k_z < 0$, where $\tilde{v}_s \equiv (\beta/\alpha - 1)v_s$.

For $h \geq 1$ the ground state of Eq. (2) is field polarized, and in the absence of spin-transfer torques, $\boldsymbol{v}_s = 0$, the static skyrmion string $\boldsymbol{n}_{\text{SkS}}(\boldsymbol{r})$ of Fig. 1(a) is a topologically stable excitation [49]. For a finite in-plane spin velocity, $\boldsymbol{v}_s \perp \hat{\boldsymbol{z}}$, the equation of motion is solved by a drifting skyrmion string $\boldsymbol{n}_{\text{SkS}}(\boldsymbol{r} - \boldsymbol{v}_d t)$ with an in-plane drift velocity $\boldsymbol{v}_d \nparallel \boldsymbol{v}_s$ realizing a skyrmion Hall effect [1].

Here, we are interested, however, in a longitudinal spin current $\boldsymbol{v}_s = v_s\hat{\boldsymbol{z}}$; as the spin-transfer torques act on the magnetization only via the operator $v_s\partial_z$ and $\partial_z \boldsymbol{n}_{\text{SkS}}(\boldsymbol{r}) = 0$, the static skyrmion string $\boldsymbol{n}_{\text{SkS}}(\boldsymbol{r})$ still solves Eq. (1). In order to determine the dynamical stability of the static string solution for $v_s \neq 0$ we perform a stability analysis by examining small fluctuations. Treating the Gilbert damping α on the right-hand side of Eq. (1) perturbatively, the complex fluctuation spectrum is obtained with the help of linear spin-wave theory, see Ref. [30] for details,

$$\omega_{v_s}(k_z) = \frac{\beta}{\alpha}v_s k_z + \left[\omega(k_z) - \left(\frac{\beta}{\alpha} - 1\right)v_s k_z\right][1 - i\alpha P(k_z)]. \tag{3}$$

Here, k_z is the wave vector of the spin wave fluctuation, and the dimensionless function $P(k_z) \geq 1$ parametrizes its

ellipticity [50,51]. For $v_s = 0$ and $\alpha = 0$, the spectrum reduces to the spin wave dispersion $\omega(k_z)$ for the skyrmion string in equilibrium that was determined before by Lin *et al.* [26], see Fig. 2(a).

The skyrmion string is dynamically stable as long as $\mathrm{Im}\{\omega_{v_s}(k_z)\} < 0$ so that the factor $e^{-i\omega_{v_s}(k_z)t}$ accompanying the fluctuation amplitude decays exponentially in time. From Eq. (3) follows the stability criterion

$$\omega(k_z) - \left(\frac{\beta}{\alpha} - 1\right) v_s k_z > 0, \tag{4}$$

that generalizes and agrees with previous work [52–55]. As the string possesses a translational Goldstone mode with a quadratic spectrum for small k_z, $\omega(k_z) \approx \mathcal{D} k_z^2$, with the stiffness $\mathcal{D}$, there exist for any value of v_s a range of wave vectors k_z for which the corresponding stability condition is not fulfilled, see Figs. 2(b) and 2(c). This implies that the string in the presence of a small longitudinal current is destabilized by the spontaneous emission of Goldstone spin waves.

With this insight, we construct from the spectrum $\omega(k_z)$ of Fig. 2(a) the instability diagram for the skyrmion string at the field $h = 2.16$, see Fig. 3(a); in Ref. [30] the diagram is also shown for $h = 1.08$. The blue shaded region bounded by the blue solid line indicates the range of wave vectors for which the translational Goldstone mode is unstable. In the limit of small k_z the blue solid line is linear, $(\beta/\alpha - 1)v_s \approx \mathcal{D} k_z$, and determined by the stiffness $\mathcal{D}$ of the Goldstone mode. Increasing the values of $(\beta/\alpha - 1)v_s$ the breathing mode, in addition, becomes unstable (red line) and, eventually, even the ground state (orange line). The latter occurs when the parabola bordering the scattering states in Figs. 2(b) and 2(c) crosses zero, $[(k_z + Q)/Q]^2 + h - 1 - k_z(\beta/\alpha - 1)v_s/\omega_{c2} = 0$; it is the mode with $k_z = \pm\sqrt{h}Q$ that becomes unstable first at the velocity $(\beta/\alpha - 1)v_s|_{\min} = 2(\pm\sqrt{h} + 1)\omega_{c2}/Q$ [56]. Because of the nonreciprocity of the spectrum, Fig. 2(a), the instability diagram lacks point symmetry with respect to the origin.

In order to validate Fig. 3(a) we performed numerical micromagnetic simulations, see Ref. [30] for details. The Goldstone amplitude spectrum of the numerically evaluated unstable skyrmion string shown in Fig. 1(b) is analyzed in the inset of Fig. 3(a). Indeed, amplitudes within the expected range of wave vectors from zero to k^*, with $\omega(k^*)/k^* = (\beta/\alpha - 1)v_s$, contribute. The imaginary part of $\omega_{v_s}(k_z)$ is maximal for a wave vector $k_{\max}$, for which the group velocity $\partial_{k_z}\omega(k_z)|_{k_{\max}} = (\beta/\alpha - 1)v_s$, and, as a consequence, this amplitude will develop the fastest. In agreement with this expectation, the amplitude spectrum has a peak close to $k_{\max}$. In order to verify the boundary of the instability region, i.e., the blue line in Fig. 3(a), we deliberately excited the string in the micromagnetic

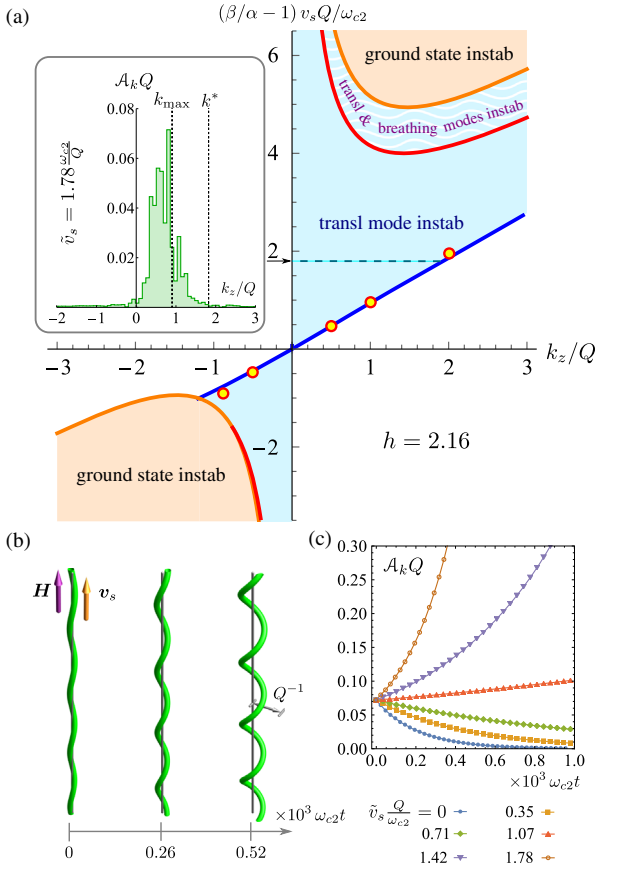

FIG. 3. (a) Instability diagram for the skyrmion string obtained with the help of Eq. (4) for a dimensionless magnetic field $h = 2.16$ and $\tilde{v}_s \equiv (\beta/\alpha - 1)v_s$. In the blue shaded region the translational Goldstone mode is unstable. The breathing mode of the string becomes unstable for larger $\tilde{v}_s$ at the red solid line. In the orange shaded region the field-polarized ground state is destabilized. Inset: Amplitude spectrum of the micromagnetic simulation displayed in Fig. 1(b), see text. (b) Micromagnetic simulations of a string initialized with a Goldstone mode at wave vector $k_z = Q$. (c) Time evolution of the corresponding amplitude that allows us to identify the critical value for $\tilde{v}_s$ indicated as yellow symbols in (a), see text.

simulations with a Goldstone mode of a given wave vector k_z and monitored the time evolution of its amplitude, see Figs. 3(b) and 3(c). Scanning various values of $(\beta/\alpha - 1)v_s$ we identified its critical value, for which the time evolution changes from an exponential decay to an exponential increase. The results for selected wave vectors are shown as yellow dots in panel (a) and are in good agreement with analytical predictions.

Now, we turn to a discussion of skyrmion string lattices realized as a stable thermodynamic phase in cubic chiral magnets with typical lattice constants of order $\sim 2\pi/Q$. Repeating the above arguments, we find that the stability criterion (4) also applies to lattices where $\omega(k_z)$ should be identified here with the spin wave spectrum at zero in-plane wave vectors, i.e., $\boldsymbol{k} = k_z \hat{\boldsymbol{z}}$. This spectrum was obtained in

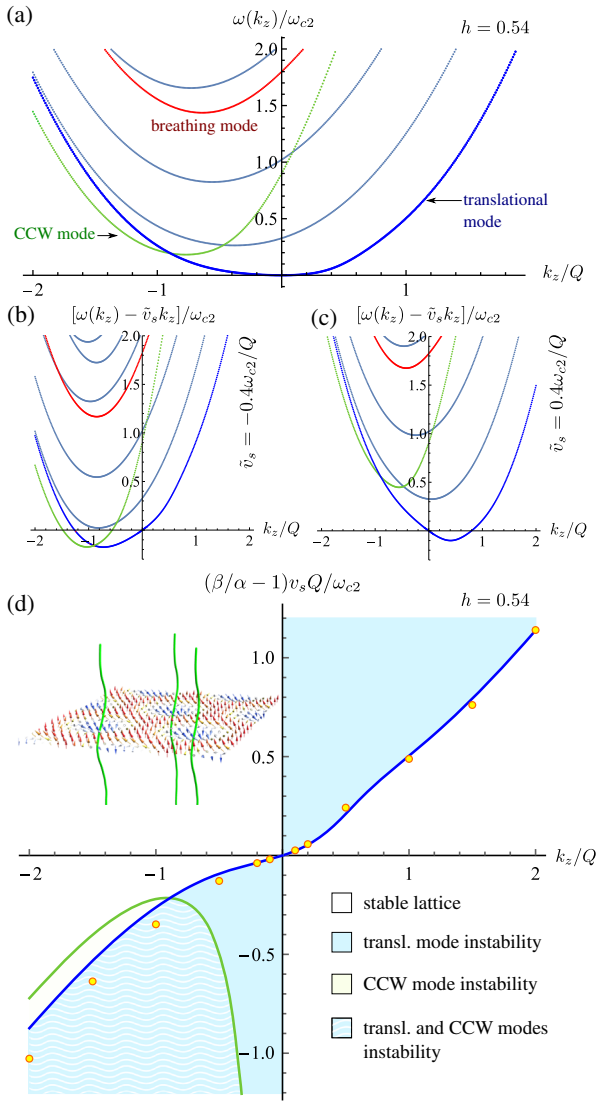

FIG. 4. (a) Magnon spectrum of the skyrmion string lattice at $h = 0.54$ for wave vectors k_z along the strings [27]. (b),(c) Violation of the stability criterion (4) in the presence of a finite $\tilde{v}_s \equiv (\beta/\alpha - 1)v_s$. (d) Instability diagram for $h = 0.54$; in the blue shaded region the Goldstone mode is unstable. At the green solid line the CCW mode also destabilizes and, subsequently, various other modes (not shown). The yellow symbols are obtained via micromagnetic simulations, see inset and text.

Ref. [27] and is shown in Fig. 4(a). It comprises various modes [19,48] but the ones with lowest frequencies are the translational Goldstone mode and the counterclockwise (CCW) mode. Similar to the case of a single string, a small applied spin current immediately destabilizes the Goldstone mode of the skyrmion string lattice, see Figs. 4(b) and 4(c). Increasing the spin current, the CCW mode, due to its pronounced nonreciprocity [27], is destabilized next for negative values of $(\beta/\alpha - 1)v_s$ and, subsequently, various other modes. This is summarized in the instability diagram of Fig. 4(d). Note that the boundary of the Goldstone instability (blue solid line) is only linear $(\beta/\alpha - 1)v_s \propto k_z$ for very small $k_z \ll Q$ due to the pronounced nonreciprocity of the Goldstone dispersion in Fig. 4(a).

Micromagnetic simulations were performed to confirm the diagram in Fig. 4(d), for details see Ref. [30]. Similar to Figs. 3(b) and 3(c), the skyrmion string lattice was initialized with a Goldstone excitation with a specific wave vector, and the time evolution was monitored to determine the critical values of the velocity, that are shown as yellow symbols in Fig. 4(d). There is very good agreement with the blue solid line obtained analytically except for larger negative values of $(\beta/\alpha - 1)v_s$. We attribute the slight deviations in this regime to the additional instability of the CCW mode that hinders a clear delineation of the Goldstone instability.

From the instability diagrams follows that even for very small spin currents the Goldstone spin wave instability is expected to develop for wave vectors $|k_z| \leq |(\beta/\alpha - 1)v_s|/\mathcal{D}$, where $\mathcal{D}$ represents the stiffness either of the single skyrmion string or the string lattice. The development will be, however, hampered if the Goldstone mode acquires an excitation gap. This is the case for a system of finite linear length L_z limiting the length of the skyrmion string; here a threshold current $v_{s,\mathrm{cr}}^{\parallel} \sim [\mathcal{D}\pi/(L_z|\beta/\alpha - 1|)]$ will be required although surface twist and anchoring effects could lead to further complications [42].

Disorder, in particular, breaks the translational symmetry and induces finite threshold currents both for longitudinal currents, $v_{s,\mathrm{cr}}^{\parallel}$, as well as for the in-plane motion of skyrmion strings due to in-plane currents, $v_{s,\mathrm{cr}}^{\perp}$. In the following, we estimate this effect assuming collective pinning by weak disorder [57]. It can be shown [30] that the two threshold velocities for a skyrmion string lattice are related by $v_{s,\mathrm{cr}}^{\parallel} \approx \sqrt{v_{s,\mathrm{cr}}^{\perp}\eta\mathcal{D}/\xi}$, where $\eta = c_{44}/c_{66}$ is the ratio of the bend and shear elastic constants of the lattice, and ξ is a length scale characterizing the disorder potential. As the size of the skyrmion is the smallest length scale that can be resolved by the string's elasticity, we approximate $\xi \sim 2\pi/Q$. From the dispersion relation for the spin waves, see Fig. 4(a) and Ref. [48], we can estimate $\mathcal{D}Q^2 \approx 0.5\omega_{c2}$ as well as $\eta \approx 0.5$. Schulz *et al.* [7] provide for a high-purity sample of MnSi a value for the critical in-plane velocity $v_{s,\mathrm{cr}}^{\perp} \sim 10^{-4}$ m/s of the skyrmion lattice motion induced by a critical charge current $j_{\mathrm{cr}}^{\perp} \sim 10^6$ A/m^2. Using $\omega_{c2}/(2\pi) = 16.7$ GHz and $2\pi/Q = 18$ nm for MnSi [48], we obtain the estimate for the longitudinal threshold velocity $v_{s,\mathrm{cr}}^{\parallel} \sim 0.03$ m/s, that is 2 orders of magnitude larger than the transversal threshold. This amounts to a critical current $j_{\mathrm{cr}}^{\parallel} \approx (v_{s,\mathrm{cr}}^{\parallel}/v_{s,\mathrm{cr}}^{\perp})j_{\mathrm{cr}}^{\perp} \sim 3 \times 10^8$ A/m^2 for the Goldstone instability in MnSi highlighting the necessity of ultrapure samples.

In summary, a spin current flowing longitudinal to magnetic skyrmion strings leads to a Goldstone spin wave instability. Its application allows, in principle, to melt the

skyrmion string lattice and induce a nonequilibrium phase transition, whose universality class, however, remains to be determined [58]. Depending on the parameters, the resulting nonequilibrium state could be either a static polarized phase, a dynamical conical state with moving phase fronts [59,60], or other dynamically ordered and disordered phases [56,61,62]. Similarly, a single skyrmion string can be topologically unwinded by longitudinal currents, which might be useful for erasing magnetic skyrmions in information storage applications [63]. As the instability mechanism is quite generic, it would be interesting to see whether other quasi-one-dimensional magnetic objects, e.g., certain domain walls, screw dislocations [64], or more complicated skyrmion strings [25,65] exhibit a similar Goldstone spin wave instability. Recently, spin wave instabilities have attracted attention in the context of magnonic black-hole analogs and spin-wave lasers [66–68]. The instability for skyrmion strings discussed here provides a potential platform to realize magnonic black-hole horizons with Goldstone modes and, consequently, relatively low threshold currents.

M. G. is supported by the Deutsche Forschungsgemeinschaft (DFG, German Research Foundation) via Project-id 403030645 and Project-id 445312953, and V. K. is partially supported by National Academy of Sciences of Ukraine (Project No. 0122U000887).

[1] N. Nagaosa and Y. Tokura, Topological properties and dynamics of magnetic skyrmions, Nat. Nanotechnol. **8**, 899 (2013).
[2] G. E. Volovik, Linear momentum in ferromagnets, J. Phys. C **20**, L83 (1987).
[3] P. Bruno, V. K. Dugaev, and M. Taillefumier, Topological Hall Effect and Berry Phase in Magnetic Nanostructures, Phys. Rev. Lett. **93**, 096806 (2004).
[4] A. Neubauer, C. Pfleiderer, B. Binz, A. Rosch, R. Ritz, P. G. Niklowitz, and P. Böni, Topological Hall Effect in the A Phase of MnSi, Phys. Rev. Lett. **102**, 186602 (2009).
[5] M. Lee, W. Kang, Y. Onose, Y. Tokura, and N. P. Ong, Unusual Hall Effect Anomaly in MnSi under Pressure, Phys. Rev. Lett. **102**, 186601 (2009).
[6] F. Jonietz, S. Muhlbauer, C. Pfleiderer, A. Neubauer, W. Munzer, A. Bauer, T. Adams, R. Georgii, P. Boni, R. A. Duine, K. Everschor, M. Garst, and A. Rosch, Spin transfer torques in MnSi at ultralow current densities, Science **330**, 1648 (2010).
[7] T. Schulz, R. Ritz, A. Bauer, M. Halder, M. Wagner, C. Franz, C. Pfleiderer, K. Everschor, M. Garst, and A. Rosch, Emergent electrodynamics of skyrmions in a chiral magnet, Nat. Phys. **8**, 301 (2012).
[8] X. Yu, N. Kanazawa, W. Zhang, T. Nagai, T. Hara, K. Kimoto, Y. Matsui, Y. Onose, and Y. Tokura, Skyrmion flow near room temperature in an ultralow current density, Nat. Commun. **3**, 988 (2012).
[9] A. Fert, V. Cros, and J. Sampaio, Skyrmions on the track, Nat. Nanotechnol. **8**, 152 (2013).
[10] J. Iwasaki, M. Mochizuki, and N. Nagaosa, Universal current-velocity relation of skyrmion motion in chiral magnets, Nat. Commun. **4**, 1463 (2013).
[11] J. Sampaio, V. Cros, S. Rohart, A. Thiaville, and A. Fert, Nucleation, stability and current-induced motion of isolated magnetic skyrmions in nanostructures, Nat. Nanotechnol. **8**, 839 (2013).
[12] W. Jiang, P. Upadhyaya, W. Zhang, G. Yu, M. B. Jungfleisch, F. Y. Fradin, J. E. Pearson, Y. Tserkovnyak, K. L. Wang, O. Heinonen, S. G. E. te Velthuis, and A. Hoffmann, Blowing magnetic skyrmion bubbles, Science **349**, 283 (2015).
[13] W. Jiang, X. Zhang, G. Yu, W. Zhang, X. Wang, M. Benjamin Jungfleisch, J. Pearson, X. Cheng, O. Heinonen, K. L. Wang, Y. Zhou, A. Hoffmann, and S. te Velthuis, Direct observation of the skyrmion Hall effect, Nat. Phys. **13**, 162 (2017).
[14] S. Woo, K. Litzius, B. Krüger, M.-Y. Im, L. Caretta, K. Richter, M. Mann, A. Krone, R. M. Reeve, M. Weigand, P. Agrawal, I. Lemesh, M.-A. Mawass, P. Fischer, M. Kläui, and G. S. D. Beach, Observation of room-temperature magnetic skyrmions and their current-driven dynamics in ultrathin metallic ferromagnets, Nat. Mater. **15**, 501 (2016).
[15] K. Litzius, I. Lemesh, B. Krüger, P. Bassirian, L. Caretta, K. Richter, F. Büttner, K. Sato, O. A. Tretiakov, J. Förster, R. M. Reeve, M. Weigand, I. Bykova, H. Stoll, G. Schütz, G. S. D. Beach, and M. Kläui, Skyrmion Hall effect revealed by direct time-resolved x-ray microscopy, Nat. Phys. **13**, 170 (2017).
[16] J. Zázvorka, F. Jakobs, D. Heinze, N. Keil, S. Kromin, S. Jaiswal, K. Litzius, G. Jakob, P. Virnau, D. Pinna, K. Everschor-Sitte, L. Rózsa, A. Donges, U. Nowak, and M. Kläui, Thermal skyrmion diffusion used in a reshuffler device, Nat. Nanotechnol. **14**, 658 (2019).
[17] K. Litzius, J. Leliaert, P. Bassirian, D. Rodrigues, S. Kromin, I. Lemesh, J. Zazvorka, K.-J. Lee, J. Mulkers, N. Kerber, D. Heinze, N. Keil, R. M. Reeve, M. Weigand, B. Van Waeyenberge, G. Schütz, K. Everschor-Sitte, G. S. D. Beach, and M. Kläui, The role of temperature and drive current in skyrmion dynamics, Nat. Electron. **3**, 30 (2020).
[18] A. Fert, N. Reyren, and V. Cros, Magnetic skyrmions: Advances in physics and potential applications, Nat. Rev. Mater. **2**, 17031 (2017).
[19] C. Back, V. Cros, H. Ebert, K. Everschor-Sitte, A. Fert, M. Garst, T. Ma, S. Mankovsky, T. L. Monchesky, M. Mostovoy, N. Nagaosa, S. S. P. Parkin, C. Pfleiderer, N. Reyren, A. Rosch, Y. Taguchi, Y. Tokura, K. von Bergmann, and J. Zang, The 2020 skyrmionics roadmap, J. Phys. D **53**, 363001 (2020).
[20] H. S. Park, X. Yu, S. Aizawa, T. Tanigaki, T. Akashi, Y. Takahashi, T. Matsuda, N. Kanazawa, Y. Onose, D. Shindo, A. Tonomura, and Y. Tokura, Observation of the magnetic flux and three-dimensional structure of skyrmion lattices by electron holography, Nat. Nanotechnol. **9**, 337 (2014).
[21] X. Yu, J. Masell, F. S. Yasin, K. Karube, N. Kanazawa, K. Nakajima, T. Nagai, K. Kimoto, W. Koshibae, Y. Taguchi, N. Nagaosa, and Y. Tokura, Real-space observation of topological defects in extended skyrmion-strings, Nano Lett. **20**, 7313 (2020).

[22] M. T. Birch *et al.*, Real-space imaging of confined magnetic skyrmion tubes, Nat. Commun. **11**, 1726 (2020).
[23] M. T. Birch, D. Cortés-Ortuño, K. Litzius, S. Wintz, F. Schulz, M. Weigand, A. Štefančič, D. A. Mayoh, G. Balakrishnan, P. D. Hatton, and G. Schütz, Toggle-like current-induced Bloch point dynamics of 3D skyrmion strings in a room temperature nanowire, Nat. Commun. **13**, 3630 (2022).
[24] D. Wolf, S. Schneider, U. K. Rößler, A. Kovács, M. Schmidt, R. E. Dunin-Borkowski, B. Büchner, B. Rellinghaus, and A. Lubk, Unveiling the three-dimensional magnetic texture of skyrmion tubes, Nat. Nanotechnol. **17**, 250 (2022).
[25] S. Seki, M. Suzuki, M. Ishibashi, R. Takagi, N. D. Khanh, Y. Shiota, K. Shibata, W. Koshibae, Y. Tokura, and T. Ono, Direct visualization of the three-dimensional shape of skyrmion strings in a noncentrosymmetric magnet, Nat. Mater. **21**, 181 (2022).
[26] S.-Z. Lin, J.-X. Zhu, and A. Saxena, Kelvin modes of a skyrmion line in chiral magnets and the associated magnon transport, Phys. Rev. B **99**, 140408(R) (2019).
[27] S. Seki, M. Garst, J. Waizner, R. Takagi, N. D. Khanh, Y. Okamura, K. Kondou, F. Kagawa, Y. Otani, and Y. Tokura, Propagation dynamics of spin excitations along skyrmion strings, Nat. Commun. **11**, 256 (2020).
[28] V. P. Kravchuk, U. K. Rößler, J. van den Brink, and M. Garst, Solitary wave excitations of skyrmion strings in chiral magnets, Phys. Rev. B **102**, 220408(R) (2020).
[29] H. Hasimoto, A soliton on a vortex filament, J. Fluid Mech. **51**, 477 (1972).
[30] See Supplemental Material at http://link.aps.org/supplemental/10.1103/PhysRevLett.131.066702, which includes Refs. [31–36], for the derivation of the fluctuation spectra, the instability criterion, the analysis of pinning by disorder, the estimate of threshold currents, and details of micromagnetic simulations.
[31] C. Schütte and M. Garst, Magnon-skyrmion scattering in chiral magnets, Phys. Rev. B **90**, 094423 (2014).
[32] A. A. Thiele, Steady-State Motion of Magnetic Domains, Phys. Rev. Lett. **30**, 230 (1973).
[33] K. Everschor, M. Garst, R. A. Duine, and A. Rosch, Current-induced rotational torques in the skyrmion lattice phase of chiral magnets, Phys. Rev. B **84**, 064401 (2011).
[34] A. Vansteenkiste, J. Leliaert, M. Dvornik, M. Helsen, F. Garcia-Sanchez, and B. Van Waeyenberge, The design and verification of MuMax3, AIP Adv. **4**, 107133 (2014).
[35] M. Beg, R. Carey, W. Wang, D. Cortés-Ortuño, M. Vousden, M.-A. Bisotti, M. Albert, D. Chernyshenko, O. Hovorka, R. L. Stamps, and H. Fangohr, Ground state search, hysteretic behaviour, and reversal mechanism of skyrmionic textures in confined helimagnetic nanostructures, Sci. Rep. **5**, 17137 (2015).
[36] S. L. Zhang, I. Stasinopoulos, T. Lancaster, F. Xiao, A. Bauer, F. Rucker, A. A. Baker, A. I. Figueroa, Z. Salman, F. L. Pratt, S. J. Blundell, T. Prokscha, A. Suter, J. Waizner, M. Garst, D. Grundler, G. van der Laan, C. Pfleiderer, and T. Hesjedal, Room-temperature helimagnetism in FeGe thin films, Sci. Rep. **7**, 123 (2017).
[37] S.-Z. Lin and A. Saxena, Dynamics of Dirac strings and monopolelike excitations in chiral magnets under a current drive, Phys. Rev. B **93**, 060401(R) (2016).
[38] F. Kagawa, H. Oike, W. Koshibae, A. Kikkawa, Y. Okamura, Y. Taguchi, N. Nagaosa, and Y. Tokura, Current-induced viscoelastic topological unwinding of metastable skyrmion strings, Nat. Commun. **8**, 1332 (2017).
[39] T. Yokouchi, S. Hoshino, N. Kanazawa, A. Kikkawa, D. Morikawa, K. Shibata, T. Arima, Y. Taguchi, F. Kagawa, N. Nagaosa, and Y. Tokura, Current-induced dynamics of skyrmion strings, Sci. Adv. **4**, eaat1115 (2018).
[40] J. Zang, M. Mostovoy, J. H. Han, and N. Nagaosa, Dynamics of Skyrmion Crystals in Metallic Thin Films, Phys. Rev. Lett. **107**, 136804 (2011).
[41] W. Koshibae and N. Nagaosa, Dynamics of skyrmion in disordered chiral magnet of thin film form, Sci. Rep. **9**, 5111 (2019).
[42] W. Koshibae and N. Nagaosa, Bulk and surface topological indices for a skyrmion string, Sci. Rep. **10**, 20303 (2020).
[43] C. Reichhardt, C. J. O. Reichhardt, and M. V. Milošević, Statics and dynamics of skyrmions interacting with disorder and nanostructures, Rev. Mod. Phys. **94**, 035005 (2022).
[44] A. Bezvershenko and A. Rosch, Walking skyrmions, Abstracts of DPG-meeting, Regensburg, 4-9 September 2022 (unpublished).
[45] Note that temperature T affects the initial string fluctuations, and the instability develops faster with increasing T, see Fig. 4 in Ref. [30].
[46] S. Zhang and Z. Li, Roles of Nonequilibrium Conduction Electrons on the Magnetization Dynamics of Ferromagnets, Phys. Rev. Lett. **93**, 127204 (2004).
[47] Y. Tserkovnyak, A. Brataas, and G. E. Bauer, Theory of current-driven magnetization dynamics in inhomogeneous ferromagnets, J. Magn. Magn. Mater. **320**, 1282 (2008).
[48] M. Garst, J. Waizner, and D. Grundler, Collective spin excitations of helices and magnetic skyrmions: Review and perspectives of magnonics in non-centrosymmetric magnets, J. Phys. D **50**, 293002 (2017).
[49] A. Bogdanov and A. Hubert, Thermodynamically stable magnetic vortex states in magnetic crystals, J. Magn. Magn. Mater. **138**, 255 (1994).
[50] V. Kambersky and C. E. Patton, Spin-wave relaxation and phenomenological damping in ferromagnetic resonance, Phys. Rev. B **11**, 2668 (1975).
[51] L. Rózsa, J. Hagemeister, E. Y. Vedmedenko, and R. Wiesendanger, Effective damping enhancement in noncollinear spin structures, Phys. Rev. B **98**, 100404(R) (2018).
[52] Y. B. Bazaliy, B. A. Jones, and S.-C. Zhang, Modification of the Landau-Lifshitz equation in the presence of a spin-polarized current in colossal- and giant-magnetoresistive materials, Phys. Rev. B **57**, R3213 (1998).
[53] J. Fernández-Rossier, M. Braun, A. S. Núñez, and A. H. MacDonald, Influence of a uniform current on collective magnetization dynamics in a ferromagnetic metal, Phys. Rev. B **69**, 174412 (2004).
[54] Y. Tserkovnyak, H. J. Skadsem, A. Brataas, and G. E. W. Bauer, Current-induced magnetization dynamics in disordered itinerant ferromagnets, Phys. Rev. B **74**, 144405 (2006).
[55] V. P. Kravchuk, Stability of magnetic nanowires against spin-polarized current, Ukr. J. Phys. **59**, 1001 (2014).
[56] S.-Z. Lin, C. Reichhardt, C. D. Batista, and A. Saxena, Driven Skyrmions and Dynamical Transitions in Chiral Magnets, Phys. Rev. Lett. **110**, 207202 (2013).

[57] G. Blatter, M. V. Feigel'man, V. B. Geshkenbein, A. I. Larkin, and V. M. Vinokur, Vortices in high-temperature superconductors, Rev. Mod. Phys. **66**, 1125 (1994).
[58] H. Hinrichsen, Non-equilibrium phase transitions, Physica (Amsterdam) **369A**, 1 (2006).
[59] N. Nagaosa, Emergent inductor by spiral magnets, Jpn. J. Appl. Phys. **58**, 120909 (2019).
[60] T. Yokouchi, F. Kagawa, M. Hirschberger, Y. Otani, N. Nagaosa, and Y. Tokura, Emergent electromagnetic induction in a helical-spin magnet, Nature (London) **586**, 232 (2020).
[61] J. Shibata, G. Tatara, and H. Kohno, Effect of Spin Current on Uniform Ferromagnetism: Domain Nucleation, Phys. Rev. Lett. **94**, 076601 (2005).
[62] J. He and S. Zhang, Magnetic dynamic phase generated by spin currents, Phys. Rev. B **78**, 012414 (2008).
[63] X. Zhang, Y. Zhou, K. M. Song, T.-E. Park, J. Xia, M. Ezawa, X. Liu, W. Zhao, G. Zhao, and S. Woo, Skyrmion-electronics: Writing, deleting, reading and processing magnetic skyrmions toward spintronic applications, J. Phys. Condens. Matter **32**, 143001 (2020).
[64] M. Azhar, V. P. Kravchuk, and M. Garst, Screw Dislocations in Chiral Magnets, Phys. Rev. Lett. **128**, 157204 (2022).
[65] J. Xia, X. Zhang, O. A. Tretiakov, H. T. Diep, J. Yang, G. Zhao, M. Ezawa, Y. Zhou, and X. Liu, Bifurcation of a topological skyrmion string, Phys. Rev. B **105**, 214402 (2022).
[66] A. Roldán-Molina, A. S. Nunez, and R. A. Duine, Magnonic Black Holes, Phys. Rev. Lett. **118**, 061301 (2017).
[67] R. J. Doornenbal, A. Roldán-Molina, A. S. Nunez, and R. A. Duine, Spin-Wave Amplification and Lasing Driven by Inhomogeneous Spin-Transfer Torques, Phys. Rev. Lett. **122**, 037203 (2019).
[68] J. S. Harms, A. Rückriegel, and R. A. Duine, Dynamically stable negative-energy states induced by spin-transfer torques, Phys. Rev. B **103**, 144408 (2021).